

# **Bovine Serum Albumin and Folic Acid-Modified Aurum Nanoparticles Loaded with Paclitaxel and Curcumin Enhance Radiotherapy Sensitization for Esophageal Cancer**

## **Authors:**

Guangyi Gao<sup>1</sup>, Wenhong Zhou<sup>1,#</sup>, Xuan Jiang<sup>1</sup>, Jun Ma<sup>2,\*</sup>

## **Affiliations:**

1 Department of Oncology, The Affiliated Huai'an Hospital of Xuzhou Medical University and The Second People's Hospital of Huai'an, Huai'an, 223002, China.

2 Department of Oncology, Huai'an TCM Hospital Affiliated to Nanjing University of Chinese Medicine, Huai'an, 223002, China.

**#These authors contributed equally.**

## **\*Corresponding Author:**

Jun Ma, Department of Oncology, Huai'an TCM Hospital Affiliated to Nanjing University of Chinese Medicine, No.3 Heping Road, qingjiangpu District, Huai'an, China. 223002. E-mail: mj1368000@163.com

## **Abstract**

**Background:** Nanocarrier systems have been used in the study of esophageal cancer (EC) and other diseases, with significant advantages in improving the non-targeted and non-specific toxicity of traditional formulations. Some chemotherapeutic drugs and high atomic number nanomaterials have sensitization effects on ionizing radiation and can be used as chemoradiation sensitizers.

**Methods:** We selected bovine serum albumin (BSA) and folic acid (FA)-modified aurum (Au) nanoparticles, which were core-loaded with paclitaxel (PTX) and curcumin (CUR). The basic characteristics of FA-BSA-Au@PTX/CUR nanomedicines were evaluated by transmission electron microscopy, Fourier transform infrared spectroscopy, and Malvern Zetasizer. The encapsulation and release of drugs were tracked by ultraviolet-visible spectrophotometry (UV-Vis). The biological toxicity and radiotherapy sensitization effect of FA-BSA-Au@PTX/CUR were observed by cell viability, colony formation, cell apoptosis, cell cycle distribution, and  $\gamma$ -H2AX analysis experiments.

**Results:** The prepared nanomedicines showed good stability and spherical morphology. The results of cell uptake and cell viability detection showed that FA-BSA-Au@PTX/CUR could specifically target EC cell KYSE150 and exert a certain inhibitory effect on proliferation, without obvious toxicity on healthy cells Het-1A. In addition, the results of colony formation experiment, cell apoptosis detection, cell cycle distribution, and  $\gamma$ -H2AX analysis showed that compared with X-rays alone, FA-BSA-Au@PTX/CUR combined with X-rays exhibited relatively stronger radiotherapy sensitization and anti-tumor activity.

**Conclusion:** FA-BSA-Au@PTX/CUR could target EC cancer cells and could be used as a safe and effective radiotherapy sensitizer to improve the radiotherapy efficacy of EC.

**Keywords:** aurum nanoparticles; bovine serum albumin; folic acid; targeting; esophageal cancer; radiotherapy sensitization

## 1. Introduction

Esophageal cancer (EC) is the seventh most common cancer and the sixth leading cause of cancer-related deaths worldwide. According to the Global Burden of Disease (GBD) statistics in 2020, one in every 18 cancer deaths is due to EC<sup>1</sup>. The occurrence of EC is often the result of multiple factors, including dietary habits, carcinogens, and genetic factors. Clinically, the main characteristic of EC patients is gradually worsening dysphagia, which can ultimately result in multiple organ failure and death due to starvation<sup>2</sup>. Although combination therapy strategies have greatly improved the prognosis of EC patients, the 5-year survival rate remains relatively low, and traditional anticancer drugs have limitations such as poor targeting, high toxicity and side effects, and short half-life, which cannot benefit all EC patients effectively<sup>3</sup>. Evidence suggests that compared with traditional formulations, nanomedicines have unparalleled advantages in cancer treatment. The clinical translation of nanomedicine may provide better treatment options for EC patients<sup>4,5</sup>.

Currently, various types of nanocarrier systems have been developed to reduce the toxic side effects of traditional chemotherapy. At the same time, some high atomic number (Z) nanomaterials (such as noble metals) have also been used as radiation sensitizers, which can enhance the efficacy of radiotherapy<sup>6</sup>. As a noble metal material, aurum (Au) nanoparticles (NPs) have good chemical stability and biocompatibility. They can not only concentrate the energy of ionizing radiation at the tumor site, showing a dose accumulation effect of radiation, but also produce more cytotoxic secondary charged particles, thus maximizing the damage of X-rays to the lesion<sup>6,7</sup>. In the study by Hainfeld *et al.*<sup>8</sup>, mice with tumors injected with Au NPs and receiving radiotherapy were substantially controlled, and most of these particles were cleared from the body through the kidneys without causing toxicity in mice.

Au NPs possess good surface modifiability and can be further used for reducing NP toxicity and improving biocompatibility *in vivo* through coating with specific protective molecules. Bovine serum albumin (BSA) is a common surface modifier for metal NPs<sup>9</sup>, and BSA-coated Au NPs (BSA-Au) have been widely used for tumor

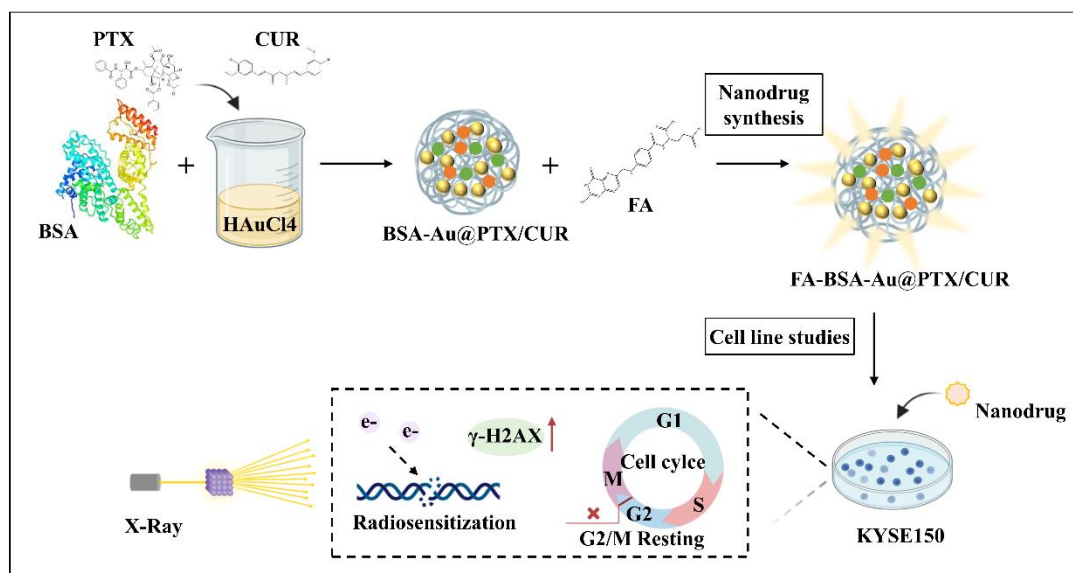
monitoring and treatment<sup>10,11</sup>. For instance, Murawala *et al.*<sup>12</sup> prepared BSA-Au NPs loaded with methotrexate (MTX) and demonstrated that BSA-Au-MTX had a more significant inhibitory effect on breast cancer cells than an equivalent dose of free MTX. Moreover, to improve the targeting effect of nanomedicines on cancer cells, folic acid (FA) can be conjugated to Au NPs due to the high expression of folate receptors (FR) on cancer cells<sup>13</sup>. In the study by Kunde *et al.*<sup>14</sup>, the antiestrogen drug, raloxifene hydrochloride (RLX), is loaded into BSA-NPs and further surface modified with FA, with the results of cell experiments showing that this complex nanomedicine has a better therapeutic effect on breast cancer than free RLX and RLX-BSA-NPs without FA modification.

Paclitaxel (PTX) is a chemotherapeutic agent extracted from the bark of the Pacific yew, which can induce cell arrest in the G2/M phase by promoting microtubule aggregation and assembly, thereby exerting an anti-tumor effect<sup>15</sup>. The G2/M phase is the most sensitive stage of the cell cycle to ionizing radiation, so drugs that can induce G2/M phase arrest are potential radiosensitizers; PTX has been shown to make various human cell lines sensitive to radiation<sup>16</sup>. Moreover, as single-drug therapy often leads to adverse reactions and poor patient compliance, some traditional Chinese medicines are often combined to relieve side effects and increase therapeutic efficacy. Curcumin (CUR) is the most representative traditional Chinese medicine, extracted from turmeric, with anti-inflammatory and anti-tumor effects. The excellent pharmacological activity of CUR has been proven to reduce the side effects of PTX<sup>17,18</sup>. We speculated that the combination of CUR and PTX had the potential to improve EC treatment.

In summary, we constructed a novel nanomedicine (FA-BSA-Au@PTX/CUR) to enhance the efficacy of EC radiotherapy by loading PTX and CUR onto BSA and FA-modified Au NPs (**Graphical abstract**). We used a simple and low-toxicity method to prepare the composite nanomedicine and systematically characterized its morphology, particle size, drug loading, and release. We also investigated the cellular uptake, cytotoxicity, and radio-sensitizing effects of FA-BSA-Au@PTX/CUR *in vitro*. From the research results, the nanomedicine prepared in this study not only exhibited good targeting to EC cells but also showed significant toxicity and radio-sensitizing effects

on EC cells, demonstrating the potential of nanomedicines in combination therapy and providing a corresponding basis for the clinical translation of nanomedicines.

**Graphical abstract: Synthesis of nanodrugs and their *in vitro* radiosensitization and anti-tumor activity.**



## 2. Materials and Methods

### 2.1 Preparation of Materials

#### 2.1.1 Preparation of BSA-Au@PTX/CUR

2 mg of PTX and 2 mg of CUR were added to 10 mL of BSA (5 mg/mL) and sonicated to dissolve. The solution was stirred at room temperature for 5 min, then 5 mL of a 10 mM H<sub>2</sub>AuCl<sub>4</sub> solution was added and stirred for 10 min. 1 mL of 1 M NaOH was added dropwise to the solution to adjust the pH to 12, and the solution was then stirred at 70 °C for 1 h. After the reaction, the material was centrifuged, washed, and freeze-dried for storage.

#### 2.1.2 Preparation of FA-BSA-Au@PTX/CUR

10 mg of FA was dissolved in 3 mL of DMSO, and then 2 mg of EDC and 3 mg of NHS were added. The mixture was stirred in the dark at room temperature for 2 h to activate the FA. Then, 20 mL of BSA-Au@PTX/CUR (1 mg/mL) was mixed with the FA solution and stirred in the dark overnight. The material was centrifuged, washed, and freeze-dried for storage.

## **2.2 Material Characterization**

The microscopic morphology of the materials was observed by transmission electron microscopy (TEM, JEM-2100, JEOL, Japan). The particle size distribution and zeta potential of the materials were analyzed using a Malvern Zetasizer Nano-ZS90 (Malvern, UK). The various functional groups of the materials were characterized by Fourier transform infrared spectroscopy (FTIR, Nicolet iS50, Thermo Scientific, USA). The drug encapsulation and release were detected using a UV-Vis spectrophotometer (UV-2450, Shimadzu, Japan).

## **2.3 *In vitro* Drug Release**

The release of PTX and CUR from FA-BSA-Au@PTX/CUR was determined using a dialysis method at different pH values (5, 7.5, and 10). 10 mg of FA-BSA-Au@PTX/CUR was dispersed in 5 mL of solution and added to a dialysis bag. The bag was then immersed in 25 mL of PBS solution at different pH values and incubated at 37 °C with shaking (100 r/min). At different time points, 1 mL of the dialysis solution was extracted, and an equal volume of fresh PBS was added to continue the release under the same conditions. The content of PTX and CUR in the dialysis solution was measured by UV-Vis.

## **2.4 Cell Experiment**

The human EC cell line KYSE150 was purchased from Tongpai Biotechnology Co., Ltd. (China), and the human esophageal epithelial cell line Het-1A was purchased from BeNa Culture Collection (China). KYSE150 cells were cultured in RPMI 1640 medium containing 10% fetal bovine serum (FBS) and 1% penicillin/streptomycin (Gibco, Life Technologies, USA), while Het-1A cells were cultured in DMEM containing 10% FBS and 1% penicillin/streptomycin. The cells were incubated at 37 °C in a humidified atmosphere containing 5% CO<sub>2</sub>.

### **2.4.1 Cellular Uptake**

Cellular uptake of the NPs was observed using a fluorescence microscope (DM4,

Leica, Germany). KYSE150 cells (or Het-1A cells) were seeded on cell slides at a density of  $1 \times 10^6$  cells/mL and incubated overnight. BSA-Au@PTX/CUR and FA-BSA-Au@PTX/CUR NPs were labeled with Sulfo-Cyanine5 (Cy5, MCE, China) at the same concentration and incubated for 4 h. The cells were washed with PBS three times. PBS without NPs was used as the control. The nuclei were stained with DAPI (Sigma, USA) for 15 min. The cells were then photographed under a fluorescence microscope.

#### **2.4.2 Cell Viability Assay**

MTT assay was performed to investigate the effect of different nanomaterials on the viability of Het-1A or KYSE150 cells, with PBS as the blank control. Het-1A and KYSE150 cells were seeded in 96-well plates at a density of  $5 \times 10^3$  cells/well and incubated at 37 °C with 5% CO<sub>2</sub> for 24 h. To compare the cytotoxicity of PTX, CUR, PTX/CUR (1:1), BSA-Au@PTX/CUR, and FA-BSA-Au@PTX/CUR systematically, different concentrations (0-12 µg/mL) of drug suspensions were added to the plates. After incubation for 48 h, MTT solution (20 µL, 5mg/mL) was added and further incubated for 4 h. The liquid in the wells was discarded, and DMSO (150 µL/well) was added to treat the cells. Finally, the absorbance ( $\lambda = 490$  nm) of cell samples was measured using microplate reader (Thermo, USA) and recorded.

To determine the effect of drugs on radiosensitization, KYSE150 cells were seeded in 96-well plates according to the above method and incubated overnight. Different concentrations of drugs were added to the plates and incubated for 24 h. The solution in the 96-well plates was discarded, and an equal amount of incomplete medium was added, followed by irradiation (Source skin distance (SSD): 100 cm, dose rate: 200 cGy/min) under a linear accelerator (Elekta, Sweden) with a single dose of 0, 2, 4, 6, and 8 Gy. The cells were then incubated for another 24 h and MTT and DMSO solutions were added, and the absorbance at 490 nm was measured using microplate reader.

#### **2.4.3 Colony Formation Assay**

KYSE150 cells were seeded in 6 cm culture dishes at an appropriate density and incubated overnight. Then, different concentrations (5, 10, and 15 µg/mL) of FA-BSA-Au@PTX/CUR nanodrugs were added to the cells. After 24 h, the culture dishes were gently washed with sterile saline to remove unabsorbed nanodrugs, and fresh culture

medium was added. The cells were then irradiated with 6-MV X-rays as soon as possible, with a single dose of 0, 2, 4, 6, and 8 Gy. Subsequently, the cells were seeded in 12-well plates at a density of 100 cells/well and incubated for 14 d. When the cell colonies became visible to the naked eye, the culture was terminated. The cells were washed twice with PBS, fixed with 75% ethanol, and stained with 5% crystal violet (MACKLIN, China). The number of colonies was counted after photographing with a camera.

#### **2.4.4 Cell Apoptosis and Cell Cycle Analysis**

KYSE150 cells ( $1 \times 10^6$  cells/well) were seeded in 6-well plates and incubated overnight. Different concentrations (5, 10, and 15  $\mu\text{g/mL}$ ) of FA-BSA-Au@PTX/CUR solution were added to the cells, which were then replaced with fresh culture medium after 24 h and irradiated with a single dose of 6 Gy X-rays. The cells were further incubated for 24 h, and the cells and supernatant were collected by centrifugation at 1000 rpm for 2 min. The cell pellets were resuspended in 100  $\mu\text{L}$  binding buffer, and the cells were stained with Annexin V-FITC/PI double staining kit (Lianke, China) and incubated in the dark at room temperature for 30 min.

For cell cycle analysis, KYSE150 cells after treatment were collected, fixed with 75% ethanol at 4 °C for 2 h, and resuspended in PBS. The cells were then centrifuged at 1500 rpm for 5 min, and the cell pellets were collected and treated with PI/RNase Staining Buffer (BD Pharmingen, USA) for 20-30 min in the dark at room temperature. The samples were detected and analyzed using a flow cytometer (Accuri C6, BD, USA).

#### **2.4.5 $\gamma$ -H2AX Assay**

We used immunofluorescence (IF) and Western blotting (WB) to detect the ionizing radiation marker  $\gamma$ -H2AX to evaluate the radiosensitization ability of nanodrugs. For IF, KYSE150 cells were incubated with nanodrugs for 12 h, followed by irradiation with 6 Gy and further incubation for 1 h. The cells were then fixed with 4% paraformaldehyde, incubated at room temperature with 0.1% Triton X-100 (Millipore, USA) for 5 min. The cells were then incubated with anti- $\gamma$ -H2AX (1:250, ab81299) overnight at 4°C. After cell rinses, samples were incubated with Fluorescein-labeled goat anti-rabbit IgG antibody (1:200, bs-0295G-AF555) for 1 h at room

temperature. The nuclei were stained with DAPI, and the cells were observed using a fluorescence microscope.

For WB, proteins were extracted from cells using RIPA lysis buffer (Thermo Scientific, USA), and protein concentrations were detected by BCA. Equal amounts of cell lysates were separated by 10% SDS-PAGE and then transferred to PVDF membranes (Amersham, USA) and sealed with 5% skim milk for 1 h at room temperature. Afterwards, membranes were incubated with anti- $\gamma$ -H2AX (1:250, ab81299) and anti-GAPDH antibody (1:5000, ab8227) overnight at 4 °C. Membranes were washed with PBS and incubated with horseradish peroxidase-labeled goat anti-rabbit IgG antibody (1:2000, ab6721) for 1 h at room temperature. Protein bands were observed using ECL detection kit (Thermo Scientific, USA). ImageJ software (v1.8.0, NIH, USA) was utilized to calculate grayscale values of the bands. All antibodies were purchased from Abcam (UK).

## 2.5 Statistical Analysis

All experiments were performed at least three times and data were presented as mean  $\pm$  standard deviation. GraphPad Prism (v8.0, La Jolla, USA) software was used to process the experimental data in this study. The differences between two groups were analyzed using *t*-test, while one-way and two-way ANOVA were used for multiple group comparisons. A *p*-value less than 0.05 was considered statistically significant (*\*p* < 0.05).

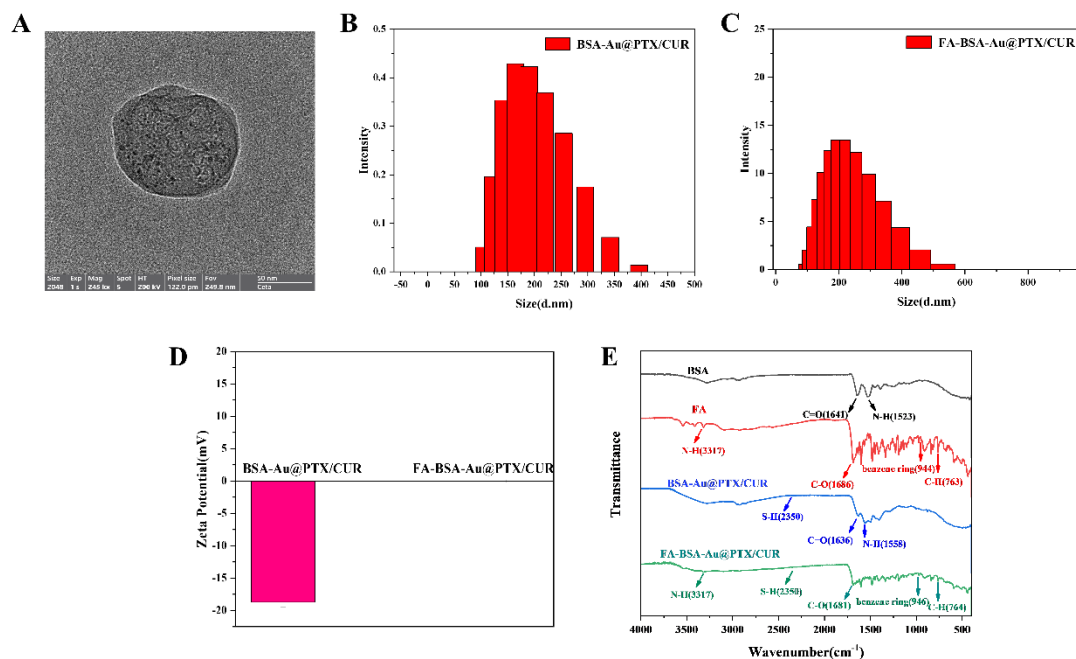
## 3. Results

### 3.1 Material Characterization

After the preparation of the materials, their structure was analyzed using TEM. As shown in **Figure 1A**, Au NPs modified with BSA and FA were formed into spherical nanomaterials of approximately 150 nm, encapsulating both PTX and CUR. Subsequently, the size and potential of BSA-Au@PTX/CUR and FA-BSA-Au@PTX/CUR were characterized using a NP size analyzer. As shown in **Figure 1B-**

**D.** The average particle size of BSA-Au@PTX/CUR and FA-BSA-Au@PTX/CUR were approximately 204 nm and 220 nm, respectively. The larger size of FA-BSA-Au@PTX/CUR was mainly due to the structural changes during the FA modification process with BSA. Furthermore, due to the FA modification, the Zeta potential of BSA-Au@PTX/CUR changed from -18.7 mV to -0.02 mV, indicating successful FA modification on the surface of BSA-Au@PTX/CUR. The drug-loaded BSA-Au@PTX/CUR and FA-modified FA-BSA-Au@PTX/CUR nanomaterials were freeze-dried and characterized using FTIR (**Figure 1E**). The spectra of BSA (black) showed characteristic peaks of BSA at 1641  $\text{cm}^{-1}$  and 1523  $\text{cm}^{-1}$ , corresponding to the stretching vibration of the amide C=O bond and the bending vibration of the amide N-H bond, respectively. The spectra of FA (red) showed characteristic peaks of FA at 3317  $\text{cm}^{-1}$ , 1686  $\text{cm}^{-1}$ , 944  $\text{cm}^{-1}$ , and 763  $\text{cm}^{-1}$ , corresponding to the stretching vibration of the primary amine N-H bond, the stretching vibration of the amide C-O bond, the benzene ring absorption peak of FA, and the bending vibration of the aromatic C-H bond, respectively. The spectra of BSA-Au@PTX/CUR (blue) showed a smaller stretching vibration peak of S-H at 2350  $\text{cm}^{-1}$ , in addition to the characteristic peaks of BSA, which confirmed the formation of Au and the connection between BSA and Au. In the spectra of FA-BSA-Au@PTX/CUR (green), all characteristic peaks of FA and BSA-Au@PTX/CUR were observed, indicating successful coupling between FA and BSA-Au@PTX/CUR. In conclusion, this study successfully prepared FA-BSA-Au@PTX/CUR nanodrugs.

**Figure 1 Characterization of the materials**

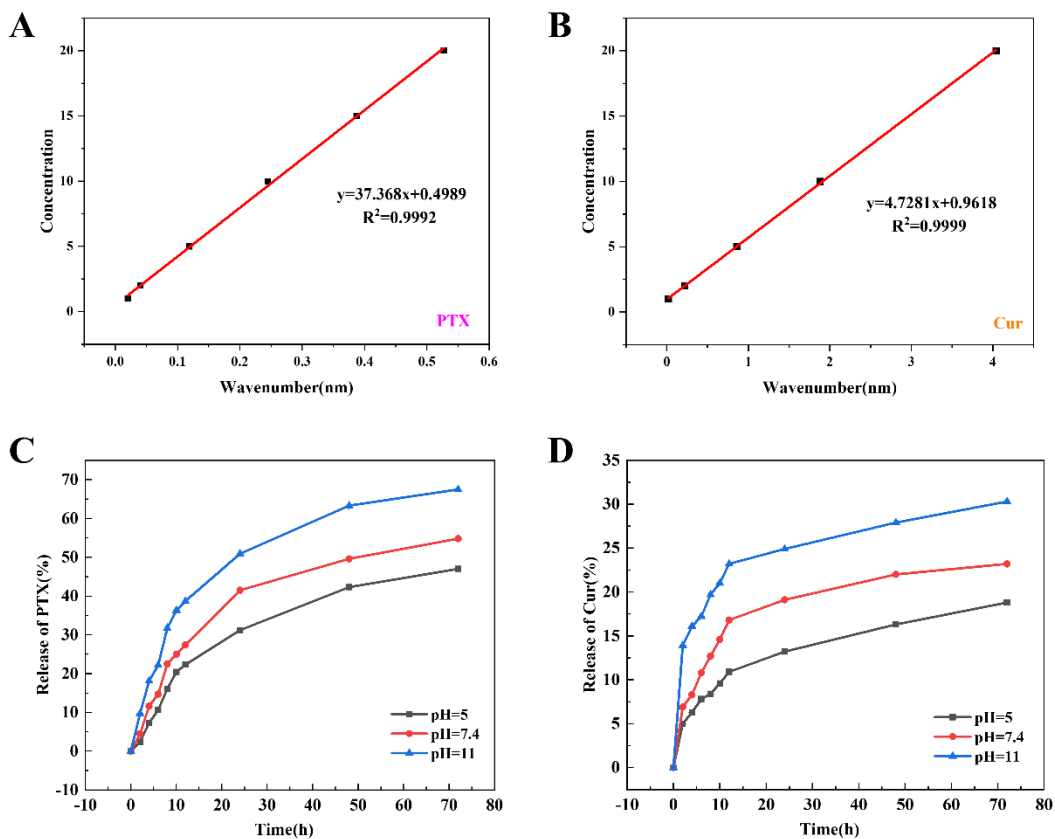


A: TEM image of BSA-Au@PTX/CUR; B-D: Particle size and Zeta potential of BSA-Au@PTX/CUR and FA-BSA-Au@PTX/CUR; E: FTIR spectra of BSA, FA, BSA-Au@PTX/CUR, and FA-BSA-Au@PTX/CUR.

### 3.2 *In vitro* Drug Release

To simulate the drug release of the nanomaterials in different environments *in vivo*, a dialysis method was used to investigate the nanomaterials under different pH conditions (5, 7.5, and 10). Based on the UV-Vis measurement of absorbance and standard curve calculation, the encapsulation efficiency and loading capacity of PTX were 52.2% and 20.3%, respectively, while those of CUR were 40.2% and 12.3%, respectively (**Figure 2A-B**). **Figure 2C** showed the drug release of PTX under different pH conditions. After 72 h, the release rate of PTX reached approximately 50% at pH 5 and 7.4, while it reached 65% at pH 11. This was mainly due to the faster decomposition of BSA at alkaline pH, which released more drugs. The drug release trend of CUR in **Figure 2D** was similar to that of PTX, and the drug release rate of CUR reached about 23% after 72 h at pH 7.4. These results indicated that the nanodrug exhibited a good response to pH values and could stably release drugs in neutral environments.

### Figure 2 Release of PTX and CUR in FA-BSA-Au@PTX/CUR



A-B: Standard curves of PTX and CUR by UV-Vis spectroscopy; C-D: Release profiles of PTX and CUR from FA-BSA-Au@PTX/CUR at different pH values (5, 7.4, 11).

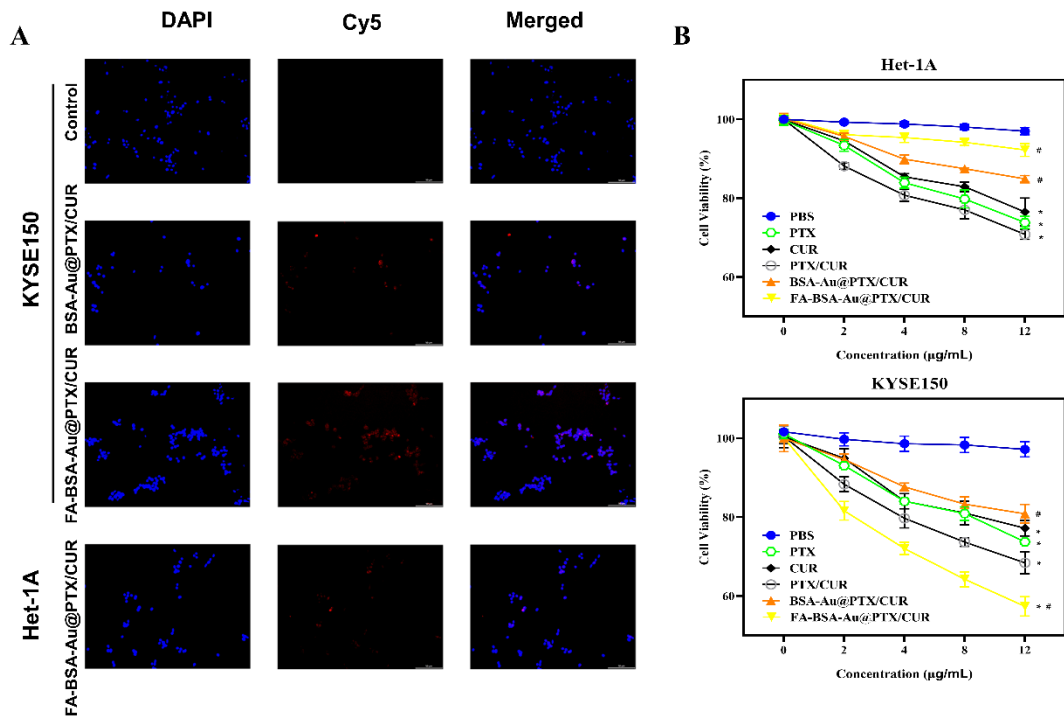
### 3.3 Cytotoxicity of the Nanodrug

Before investigating the toxicity of FA-BSA-Au@PTX/CUR, we first conducted a cell uptake experiment to evaluate whether the nanodrug could target cancer cells and be effectively taken up by them. As depicted in **Figure 3A**, after incubation with Het-1A cells, the NPs that entered Het-1A cells were relatively small due to the low expression of FA receptors in Het-1A cells, resulting in weak red fluorescence intensity. In contrast, in KYSE150 cells, compared with the blank control group, both BSA-Au@PTX/CUR and FA-BSA-Au@PTX/CUR displayed certain fluorescence, and the fluorescence intensity of the FA-BSA-Au@PTX/CUR group was much higher than that of the BSA-Au@PTX/CUR group. This was because FA could specifically recognize the FA receptor on the surface of cancer cells, mediating the phagocytosis of nanodrugs, while the amount of BSA-Au@PTX/CUR without FA modification entering cancer

cells was relatively low. These experimental results indicated that FA modification could promote the effective entry of nanodrugs into cancer cells.

To test the effects of different (nano)drugs on the viability of Het-1A or KYSE150 cells, we conducted an MTT assay. As shown in **Figure 3B**, with the increase in drug concentration, PTX, CUR, or the synergistic effect of the two drugs all significantly affected the viability of Het-1A cells. However, BSA-Au@PTX/CUR showed low toxicity to cells, and both the PBS and FA-BSA-Au@PTX/CUR groups showed no significant toxicity to Het-1A cells, indicating that the synthesized FA-BSA-Au@PTX/CUR nanodrug had good biocompatibility. In KYSE150 cells, compared with the PBS control, PTX, CUR, PTX/CUR, BSA-Au@PTX/CUR, and FA-BSA-Au@PTX/CUR all inhibited the viability of KYSE150 cells with increasing drug concentrations. However, the inhibitory effect of FA-BSA-Au@PTX/CUR nanodrug was the most significant, and its anticancer effect had a drug concentration-dependent characteristic. Therefore, compared with free PTX, CUR, or PTX/CUR, the use of FA-BSA-Au@PTX/CUR nanocarrier to deliver both drugs simultaneously effectively enhanced the inhibitory effect of drugs on KYSE150 cells and avoided affecting the activity of normal cells.

**Figure 3 Preferential uptake of FA-modified nanodrugs by cancer cells and significant inhibition of cancer cell viability**

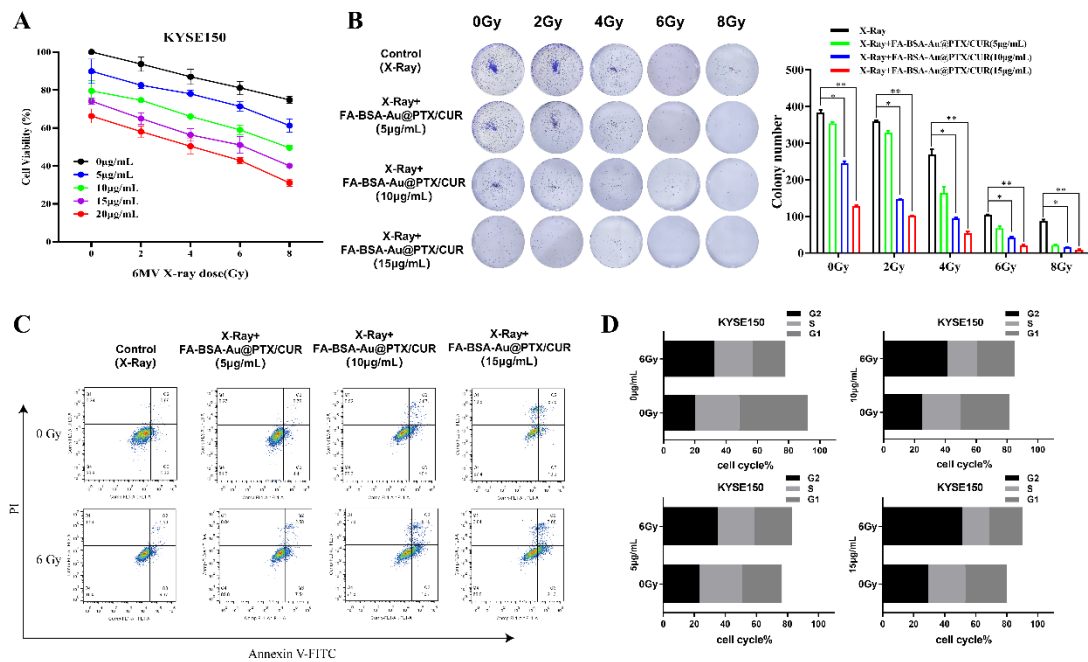


A: Fluorescence images of Het-1A/KYSE150 cells co-incubated with Cy5-labeled FA-BSA-Au@PTX/CUR or BSA-Au@PTX/CUR for 4 h; B: Cell viability of Het-1A and KYSE150 cells co-incubated with drugs at different concentrations for 48 h (\* compared with PBS, # compared with PTX/CUR, \* and # indicate  $p < 0.05$ ).

### 3.4 *In vitro* Antitumor and Radiosensitizing Effects

To evaluate the *in vitro* antitumor and radiosensitizing effects of FA-BSA-Au@PTX/CUR, we studied the effects of different concentrations (0, 5, 10, 15, 20 µg/mL) of FA-BSA-Au@PTX/CUR and different doses (0, 2, 4, 6, and 8 Gy) of X-ray radiation on cell viability. As illustrated in **Figure 4A**, cell viability gradually decreased with increasing radiation dose and FA-BSA-Au@PTX/CUR concentration. Furthermore, we used colony formation assay to explore the effect of FA-BSA-Au@PTX/CUR on KYSE150 cells. As presented in **Figure 4B**, compared with the X-ray alone group, the combination of FA-BSA-Au@PTX/CUR and radiation showed a decreased colony formation, and the inhibitory effect on colonies was more significant at higher concentrations, indicating that cell survival rate decreased with increasing radiation dose and FA-BSA-Au@PTX/CUR concentration. Additionally, we found that FA-BSA-Au@PTX/CUR could significantly enhance the killing ability of X-rays. Cell

apoptosis and cell cycle distribution were important indicators for evaluating the *in vitro* antitumor effect of nanodrugs. As shown in **Figure 4C**, with the increase in FA-BSA-Au@PTX/CUR concentration and radiation dose, the apoptosis rate also increased. The difference in cell cycle distribution among the groups was mainly manifested as an increase in the percentage of G2/M phase cells with increasing NP concentration and radiation dose, and no significant difference was observed in the S phase (**Figure 4D**). **Figure 4** *In vitro* anti-tumor and radiosensitization effects of FA-BSA-Au@PTX/CUR

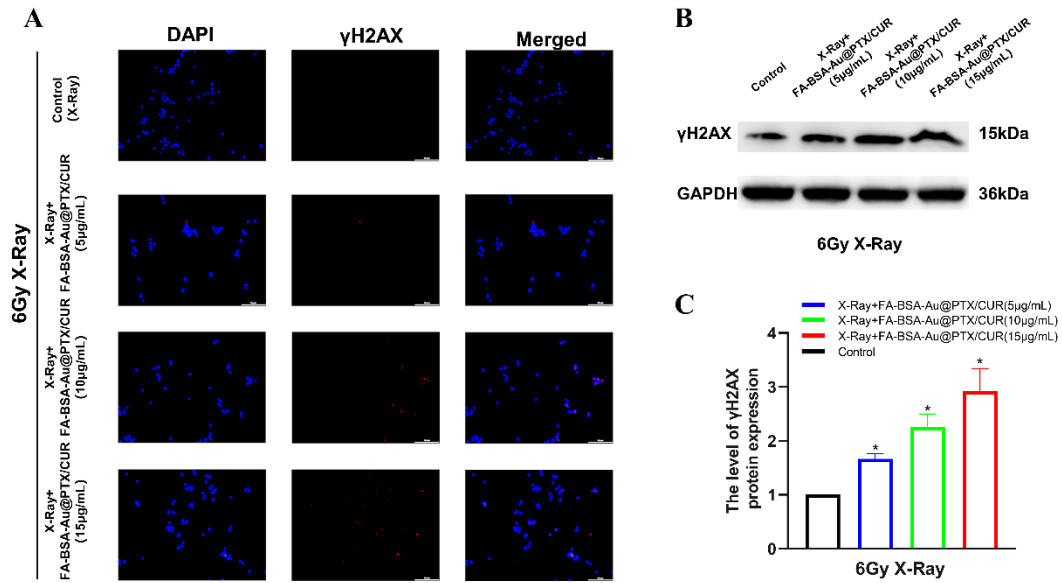


A: Cell viability of KYSE150 cells treated with different concentrations of FA-BSA-Au@PTX/CUR in combination with different doses of 6MV X-rays; B: Colony formation of cells treated with X-rays alone or in combination with different concentrations of FA-BSA-Au@PTX/CUR (\*  $p < 0.05$ , \*\*  $p < 0.01$ , \*\*\*  $p < 0.001$ ); C-D: Cell apoptosis and cell cycle distribution of different treatment groups.

In addition, we also used IF and WB to detect the  $\gamma$ H2AX levels of cells treated with different concentrations of FA-BSA-Au@PTX/CUR under 6Gy X-ray radiation conditions to evaluate the degree of DNA damage. As plotted in **Figure 5**, compared with X-ray alone, the addition of FA-BSA-Au@PTX/CUR nanodrug resulted in more severe DNA damage, which increased with increasing drug concentration, indicating

that the nanodrug made KYSE150 cells more sensitive to ionizing radiation. These results suggested that FA-BSA-Au@PTX/CUR may be an effective radiosensitizer for *in vitro* treatment of EC.

**Figure 5 FA-BSA-Au@PTX/CUR sensitizes KYSE150 cells to ionizing radiation**



A: Fluorescence microscopy images of  $\gamma$ H2AX foci in different treatment groups; B-C: WB analysis of  $\gamma$ H2AX levels in different treatment groups (\*  $p < 0.05$ ).

#### 4. Discussion

EC is a common malignancy that threatens human health, and clinical treatments mainly involve comprehensive approaches, such as surgery, radiotherapy, and chemotherapy. However, traditional chemotherapy drugs may have drawbacks such as non-selectivity and poor utilization efficiency, and radiotherapy usually requires high doses of ionizing radiation, which can cause varying degrees of toxic side effects to patients. With the advancement of nanomedicine, people attempt to use nanomaterials to deliver drugs, in order to enhance drug targeting, bioavailability, and reduce toxicity, and some chemotherapy drugs and high-Z elements can be used as radiosensitizers to improve the efficacy of radiotherapy. Based on this background, this study designed and prepared a new type of nanodrug, FA-BSA-Au@PTX/CUR, to target deliver both PTX and CUR drugs, and enhance cancer cell sensitivity to ionizing radiation, thus

helping to improve the treatment of EC patients.

The radiosensitizing ability of PTX and Au NPs has been previously reported. As a chemotherapy drug, PTX can prevent the formation of the spindle during mitosis by microtubules, causing cells to arrest in the G2/M phase, which is the most sensitive stage of the cell cycle to ionizing radiation, therefore, PTX can also be used as a radiosensitizer<sup>15,16</sup>. In addition, we also combined a natural compound, CUR, for the synergistic treatment of EC, with many studies supporting the synergistic effect between the two drugs. For example, Nguyen *et al.*<sup>19</sup> prepared a nano-gel carrier loading PTX and CUR through a hydrophobic core and verified through experiments that the drug is indeed more effective in inhibiting cancer cells than free PTX *in vitro*. This is in line with the results of the cell viability experiment in this study, and the modified Au NPs not only simultaneously loaded PTX and CUR but also enhanced the targeting ability and radiosensitizing effect on cancer cells.

Au NPs, as a high-Z element material, can accumulate ionizing radiation at the tumor site, allowing the same dose of X-rays to have a better effect on lesion damage<sup>6,7</sup>. For example, in Mochizuki *et al.*'s study, Au NPs (OS/Au) are surface functionalized with organic silicon NPs (OS) to synthesize effective Au materials as X-ray sensitizers, which can synergize with radiotherapy to inhibit the proliferation of mouse breast cancer cells and induce cell death<sup>20</sup>. In recent years, many studies have been carried out to apply different Au-based nanomaterials to tumor therapy, and after modification, these NPs exhibit good biocompatibility in circulation and can be metabolized by the liver and kidneys<sup>8</sup>. In this study, BSA and FA were used to modify Au NPs. According to the results of cell uptake and cell viability tests, FA-BSA-Au@PTX/CUR was mainly taken up by KYSE150 cells and not normal Het-1A cells. Moreover, the impact of the nanodrug on the survival of normal cells was weak, only exerting a toxic effect on cancer cells. Compared with using a single X-ray, after applying ionizing radiation, FA-BSA-Au@PTX/CUR inhibited the proliferation of KYSE150 cells, promoted cell apoptosis and DNA damage, and significantly inhibited the cell cycle at the G2/M phase. These effects became more significant with the increase of FA-BSA-Au@PTX/CUR concentration, indicating that the FA-BSA-Au@PTX/CUR prepared in this study was

a safe and effective radiosensitizer, which may synergize with radiotherapy to increase treatment efficacy.

In summary, this study successfully prepared the FA-BSA-Au@PTX/CUR composite nanodrug based on Au NPs and systematically characterized its morphology, particle size, and stability, etc. After FA and BSA modification, the drug showed good biocompatibility and low toxicity to normal cells. *In vitro* experiments demonstrated that FA-BSA-Au@PTX/CUR, when used in combination with X-rays, could effectively increase the radiotherapy damage to cancer cells. However, there are still certain limitations to the current experiments, such as the lack of pharmacokinetic research and animal model verification, etc. In the future, we will further track the distribution and metabolism of nanodrugs in the body and explore more accurate and efficient drug concentration effects. Overall, our study provides a safe and feasible radiosensitizer to promote radiotherapy for EC, and we hope that such research can accelerate the clinical application of nanodrugs.

## **Declarations:**

### **Author contribution**

GY G and WH Z conceived of the study, and participated in its design and interpretation and helped to draft the manuscript. X J participated in the design and interpretation of the data and drafting/revising the manuscript. J M performed the statistical analysis and revised the manuscript critically. All the authors read and approved the final manuscript.

### **Conflict of Interests**

The authors have no conflicts of interest to declare.

### **Data Availability Statement**

The data and materials in the current study are available from the corresponding author on reasonable request.

### **Funding**

This work was supported by Huai'an City Health and Health Scientific Research Project, No. HAWJ202114. Study of iRGD combined with metformin-loaded erythrocyte

membrane nanoparticles increasing radiotherapy sensitivity in esophageal cancer, 2022/01-2023/12.

### **Ethics approval and consent to participate**

Not applicable.

### **References**

- 1 Sung, H. *et al.* Global Cancer Statistics 2020: GLOBOCAN Estimates of Incidence and Mortality Worldwide for 36 Cancers in 185 Countries. *CA Cancer J Clin* **71**, 209-249, doi:10.3322/caac.21660 (2021).
- 2 Uhlenhopp, D. J., Then, E. O., Sunkara, T. & Gaduputi, V. Epidemiology of esophageal cancer: update in global trends, etiology and risk factors. *Clin J Gastroenterol* **13**, 1010-1021, doi:10.1007/s12328-020-01237-x (2020).
- 3 Li, X. *et al.* The development and progress of nanomedicine for esophageal cancer diagnosis and treatment. *Semin Cancer Biol* **86**, 873-885, doi:10.1016/j.semcancer.2022.01.007 (2022).
- 4 Zhan, W. *et al.* Construction of Biocompatible Dual-Drug Loaded Complicated Nanoparticles for in vivo Improvement of Synergistic Chemotherapy in Esophageal Cancer. *Front Oncol* **10**, 622, doi:10.3389/fonc.2020.00622 (2020).
- 5 Pavitra, E. *et al.* Engineered nanoparticles for imaging and drug delivery in colorectal cancer. *Semin Cancer Biol* **69**, 293-306, doi:10.1016/j.semcancer.2019.06.017 (2021).
- 6 Schuemann, J. *et al.* Roadmap to Clinical Use of Gold Nanoparticles for Radiation Sensitization. *Int J Radiat Oncol Biol Phys* **94**, 189-205, doi:10.1016/j.ijrobp.2015.09.032 (2016).
- 7 Song, G., Cheng, L., Chao, Y., Yang, K. & Liu, Z. Emerging Nanotechnology and Advanced Materials for Cancer Radiation Therapy. *Adv Mater* **29**, doi:10.1002/adma.201700996 (2017).
- 8 Hainfeld, J. F., Slatkin, D. N. & Smilowitz, H. M. The use of gold nanoparticles to enhance radiotherapy in mice. *Phys Med Biol* **49**, N309-315, doi:10.1088/0031-9155/49/18/n03 (2004).
- 9 Chu, Z. *et al.* Ultrasmall Au-Ag Alloy Nanoparticles: Protein-Directed Synthesis, Biocompatibility, and X-ray Computed Tomography Imaging. *ACS Biomater Sci Eng* **5**, 1005-1015, doi:10.1021/acsbomaterials.8b01176 (2019).
- 10 Wei, J., Li, P., Zhang, H. & Zhu, R. Preparation of BSA-coated Au Nanoparticles Contrast Agent and Its Application in PETCT Imaging. *Cell Mol Biol (Noisy-le-grand)* **68**, 158-170, doi:10.14715/cmb/2022.68.3.19 (2022).
- 11 Zu, L., Liu, L., Qin, Y., Liu, H. & Yang, H. Multifunctional BSA-Au nanostars for photoacoustic imaging and X-ray computed tomography. *Nanomedicine* **12**, 1805-1813, doi:10.1016/j.nano.2016.05.003 (2016).
- 12 Murawala, P., Tirmale, A., Shiras, A. & Prasad, B. L. In situ synthesized BSA capped gold nanoparticles: effective carrier of anticancer drug methotrexate to MCF-7 breast cancer cells. *Mater Sci Eng C Mater Biol Appl* **34**, 158-167, doi:10.1016/j.msec.2013.09.004 (2014).
- 13 Narmani, A. *et al.* Folic acid functionalized nanoparticles as pharmaceutical carriers in drug

- delivery systems. *Drug Dev Res* **80**, 404-424, doi:10.1002/ddr.21545 (2019).
- 14 Sinai Kunde, S. & Wairkar, S. Folic acid anchored urchin-like raloxifene nanoparticles for receptor targeting in breast cancer: Synthesis, optimisation and in vitro biological evaluation. *Int J Pharm* **623**, 121926, doi:10.1016/j.ijpharm.2022.121926 (2022).
- 15 Safran, H. & Rathore, R. Paclitaxel as a radiation sensitizer for locally advanced pancreatic cancer. *Crit Rev Oncol Hematol* **43**, 57-62, doi:10.1016/s1040-8428(01)00184-6 (2002).
- 16 Sikov, W. M. & Safran, H. Weekly paclitaxel as a radiation sensitizer for locally advanced gastric and pancreatic cancers: the Brown University Oncology Group experience. *Front Biosci* **2**, e21-27, doi:10.2741/a222 (1997).
- 17 Giordano, A. & Tommonaro, G. Curcumin and Cancer. *Nutrients* **11**, doi:10.3390/nu11102376 (2019).
- 18 Ashrafizadeh, M. *et al.* Curcumin in cancer therapy: A novel adjunct for combination chemotherapy with paclitaxel and alleviation of its adverse effects. *Life Sci* **256**, 117984, doi:10.1016/j.lfs.2020.117984 (2020).
- 19 Nguyen, N. T. *et al.* Curcumin and Paclitaxel Co-loaded Heparin and Poloxamer P403 Hybrid Nanocarrier for Improved Synergistic Efficacy in Breast Cancer. *Curr Drug Deliv* **19**, 966-979, doi:10.2174/1567201819666220401095923 (2022).
- 20 Mochizuki, C. *et al.* Surface Functionalization of Organosilica Nanoparticles With Au Nanoparticles Inhibits Cell Proliferation and Induces Cell Death in 4T1 Mouse Mammary Tumor Cells for DNA and Mitochondrial-Synergized Damage in Radiotherapy. *Front Chem* **10**, 907642, doi:10.3389/fchem.2022.907642 (2022).